Synthesis of Observations from the Precision Atmospheric Marine Boundary Layer Experiment (PreAMBLE)

DAVID A. RAHN

Department of Geography and Atmospheric Science, University of Kansas, Lawrence, Kansas

THOMAS R. PARISH AND DAVID LEON

Department of Atmospheric Science, University of Wyoming, Laramie, Wyoming

(Manuscript received 27 September 2016, in final form 7 March 2017)

ABSTRACT

Research flights during the Precision Atmospheric Marine Boundary Layer Experiment (PreAMBLE) in Southern California during May–June 2012 focused on three main features found in the nearshore marine boundary layer (MBL): the coastal jet (10 flights), the Catalina eddy (3 flights), and the initiation of a southerly surge (1 flight). Several topics were examined with case studies, but results from individual events may not represent typical conditions. Although these flights do not constitute a long-term set of data, observations from PreAMBLE are used to find common features. Two main topics are addressed: the MBL collapse into the expansion fan, and the subsequent transition into the Santa Barbara Channel (SBC). The midmorning to late afternoon flights occur during moderate to strong northerly wind. Slope of the MBL in the expansion fan varies and wave perturbations can be embedded within the expansion fan. As the cool MBL flow turns into the SBC, it moves underneath a deeper and warmer MBL that originates from the southeast over the warmer ocean. The temperature inversion between the cool and warm MBL erodes toward the east until there is only the inversion between the warm MBL and free troposphere. The dissipation of the lower layer into the SBC observed by the aircraft differs from previous conceptual models that depict a continuous MBL that thins and then deepens again in the SBC, which was inferred from sparse observations and numerical simulations. Only one flight within the SBC detected a hydraulic jump from 100 to 200 m above the surface.

1. Introduction

The Precision Atmospheric Marine Boundary Layer Experiment (PreAMBLE) was a field study conducted from 16 May to 16 June 2012 based out of the Naval Air Station at Point Mugu, California (see Fig. 1 for geographic locations). The primary focus of PreAMBLE was a detailed examination of the atmospheric dynamics near the Point Arguello and Point Conception headlands (PAPC) and into the California bight using the University of Wyoming King Air research aircraft as the principal measurement platform. Airborne observations of the lower atmosphere offshore of Southern California are rare since they are difficult to obtain, in part due to military air space restrictions.

Fifteen research flights totaling 48 h occurred over the month-long deployment and primarily targeted the coastal jet near PAPC, the Catalina eddy, or the initiation of a southerly surge. The Catalina eddy is a cyclonic mesoscale circulation that is typically accompanied by an anomalously deep marine boundary layer (MBL), which is associated with improved air quality in the Los Angeles basin (Wakimoto 1987). A southerly surge occurs when the normal northerly wind regime is interrupted by southerly wind that is usually accompanied with fog or low stratus that surges to the north along the coast (Nuss et al. 2000). Southerly surges are also referred to as wind reversals, coastally trapped wind reversals, or coastally trapped disturbances. The high frequency of coastal jets near PAPC in May and June practically ensured that a coastal jet would occur during PreAMBLE. Capturing a well-developed Catalina eddy or southerly surge was less certain because they are much less frequent. No detailed airborne case studies of a Catalina eddy had been completed to date. The expectation was that only a handful of strong coastal jets

Corresponding author: David A. Rahn, darahn@ku.edu

DOI: 10.1175/MWR-D-16-0373.1

© 2017 American Meteorological Society. For information regarding reuse of this content and general copyright information, consult the AMS Copyright Policy (www.ametsoc.org/PUBSReuseLicenses).

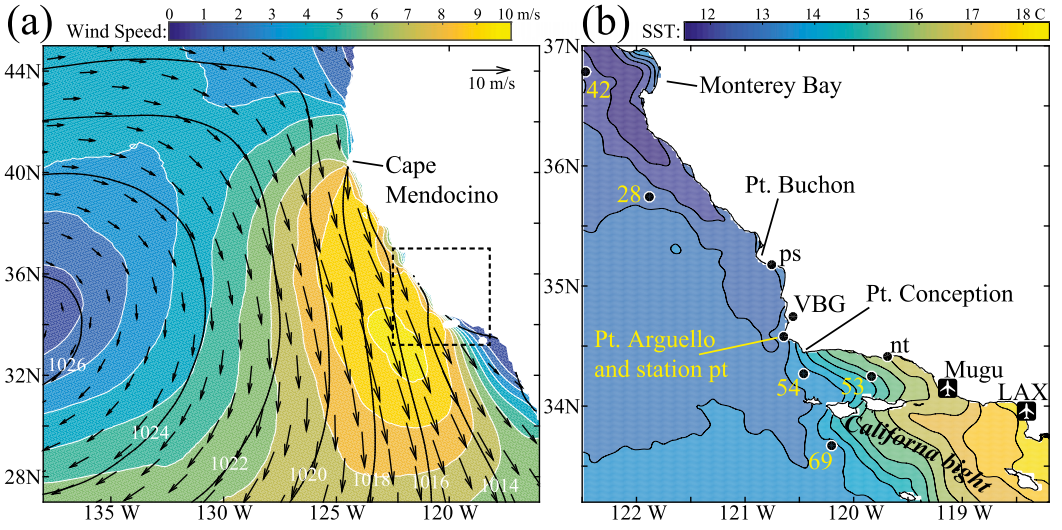

FIG. 1. (a) Average mean sea level pressure (hPa, contours) and daily 10-m wind vectors ($m\,s^{-1}$) during PreAMBLE (16 May–16 Jun 2012) obtained from the NAM 218-grid analysis. (b) Average SST (color and contoured every 0.5°C) from the Global 1-km Sea Surface Temperature (G1SST) product (Chao et al. 2009, http://ourocean.jpl.nasa.gov/SST). The dots indicate locations of buoy and surface station observations. Pertinent geographic locations identified. The domain of (b) is indicated by the dashed box in (a).

would be observed and that there was only a small chance of either a Catalina eddy or southerly surge occurring during PreAMBLE, but the conditions during the field project were exceptional resulting in measurements of all three phenomena.

A series of case studies from PreAMBLE has already been published. Although case studies are excellent for a thorough analysis of a single event, individual events do not address the generality of the findings. Here, the variety of cases that occurred throughout the month-long field campaign is synthesized and assessed in a more comprehensive approach than a single case study. In addition to presenting conditions during the field campaign and encapsulating major features of all flights during PreAMBLE, there are two main topics that are the focus of this analysis. The first topic addresses the range of finescale structures of the MBL collapse into the expansion fan in the lee of PAPC. The second topic makes use of the 90 vertical profiles of temperature, humidity, and wind components obtained in the Santa Barbara Channel (SBC) as the aircraft ferried between Point Mugu and PAPC to understand the transition of the expansion fan into the SBC. The vertical structure observed in the SBC was different from previous conceptual models (e.g., Dorman and Koračin 2008), and we will propose a slightly modified conceptual model within the SBC that was commonly encountered during PreAMBLE.

Although previous case studies have had some success in simulating the conditions near Point Conception (e.g., Parish et al. 2014), model results within the SBC tend to inadequately represent the subtle layering that regularly appeared in the lidar backscatter and in situ measurements (Rahn et al. 2014). Thus, model data are not considered here. A discussion on the meteorological background of the region and the conditions at the surface and in the lower atmosphere during PreAMBLE is presented in the following section. Section 3 provides a synthesis of the measurements. The main focus is on the collapse of the MBL near PAPC and the transition further into the SBC. The results are summarized in section 4.

2. Conditions during PreAMBLE

a. *Meteorological background*

The summertime MBL and wind field off the West Coast of the United States is normally controlled by the Pacific high and the thermal low in the desert Southwest. Isobars of the mean sea level pressure over the eastern Pacific adjacent to the coast are oriented parallel to the coastline and winds in the MBL are predominantly from the northwest and follow the coast. The top of the MBL is marked by a strong temperature inversion maintained by subsidence above the Pacific high. The MBL is deeper offshore and the steepest slope of MBL height is near the coast (Beardsley et al. 1987). A distinct low-level jet is often found at the top of the MBL and wind speeds in excess of $25\,m\,s^{-1}$ have been observed (Zemba and Friehe 1987; Burk and Thompson 1996; Rogers et al. 1998;

Parish 2000; Pomeroy and Parish 2001; Rahn and Parish 2007).

An extensive body of literature is devoted to the impact of coastal topography on the winds off the California coast. Flow in the MBL is bounded to the east by the coastal mountain range that is generally above the top of the MBL. Studies often represent the fluid system near the coast in terms of a two-layer shallow-water model with the coastal terrain serving as a lateral boundary (Dorman 1985; Winant et al. 1988; Samelson 1992; Dorman et al. 1999; Burk et al. 1999; Haack et al. 2001). Thus, the key diagnostic in this fluid system is the shallow-water Froude number, which is the ratio of the mean wind in the MBL to the fastest possible gravity wave in the MBL. For a Froude number greater than one (supercritical), gravity waves cannot propagate upstream. Since flows are often transcritical (Froude number between 0.5 and 1) or supercritical, hydraulic features can form along the coast. Expansion fans form at convex bends in the coastline where the flow in the MBL diverges, the MBL thins, and the wind speed increases. Compression bulges form at concave bends in the coastline where the flow in the MBL converges, deepens, and the wind speed decreases. The most abrupt change in the California coastline occurs at PAPC. Numerical modeling work by Dorman and Koračin (2008) outlined key issues for the atmospheric dynamics near PAPC; their results support the importance of hydraulic dynamics in the MBL.

b. *Surface features during PreAMBLE*

The analysis fields from the National Centers for Environmental Prediction's (NCEP's) North American Mesoscale Forecast System (NAM) on the 218 grid (~12-km grid spacing) depict the synoptic conditions. The NAM analysis data are archived on the NCDC National Operational Model Archive and Distribution System (NOMADS) website (nomads.ncdc.noaa.gov/data.php). During PreAMBLE, there is a maximum in the average 10-m wind speed located off of the Southern California coast centered at about the same latitude as the SBC (Fig. 1a). The northern extent of the higher wind speeds was near Cape Mendocino and the modulation of wind by the coastline is evident by the presence of local extrema in wind speed near coastal points and bays. Since the system is well represented by shallow-water flow, the wind maxima and minima along the coast are typically interpreted as expansion fans and compression bulges, respectively (Koračin and Dorman 2001). Within the California bight, the wind speed decreases toward the east. Wind direction is primarily alongshore for much of the California coast, and the wind turns more westward within the bight. The alongshore wind stress on the ocean surface near the coast induces offshore Ekman transport of the upper ocean layer and induces coastal upwelling of the cooler water from below. The cooler sea surface temperatures (SSTs) associated with the coastal upwelling is clear in Fig. 1b and farther into the California bight, the SST warms considerably.

Many features that appear in the mean state exhibit little variation during the field campaign. Hourly buoy observations during PreAMBLE reveal little directional variability in the wind near PAPC and in the SBC (Fig. 2). At buoy 54, 92% of the wind directions are from the northwest quadrant with an average wind speed of $9.2\,m\,s^{-1}$. The average wind speed during PreAMBLE was higher than the 2007–15 average over the same time of year, which was $7.9\,m\,s^{-1}$. Buoy 53 in the SBC exhibits more variability and has an average wind speed of $4.0\,m\,s^{-1}$ at 264°; 86% of the wind directions have a positive zonal wind component (winds from the west).

The average diurnal cycle of surface wind measurements during PreAMBLE is examined using temporal hodographs at several buoy[1] and coastal surface stations (Fig. 2a). The temporal hodograph is created from the mean wind at each hour of the day (in UTC time). The hourly mean is plotted with an open circle every 3 h and labeled every 6 h with a line break between 2300 and 0000 UTC. There is a clear diurnal cycle with the highest wind speeds during the late afternoon to early evening over all locations (Fig. 2a). Considerable differences appear in the average diurnal low-level wind along the coast. The least diurnally variable low-level wind is found north of PAPC at buoys 28 and 42. In the lee of PAPC, the coastal jet wind speed maxima is represented at buoy 54, similar to Dorman and Winant (2000), and exhibits a nearly circular diurnal cycle. The low-level flow at coastal station pt located at Point Arguello is relatively strong and meridional with a weak easterly component, likely due to the adjacent topography. South-southeast (SSE) of PAPC, buoy 69 exhibits a similar circular diurnal pattern, though slightly weaker. Diurnal variability of the wind in the SBC is notably different. At buoy 53 the mean wind is westerly with a weak southerly component. The temporal hodograph indicates primarily zonal changes. These temporal hodographs reveal that the mean wind is influenced by the nearby coastal topography and that the wind undergoes a marked diurnal cycle (Dorman and Koračin 2008). Previous conceptual models have relied primarily

[1] Wind measurements at buoy 11 were not functioning during PreAMBLE.

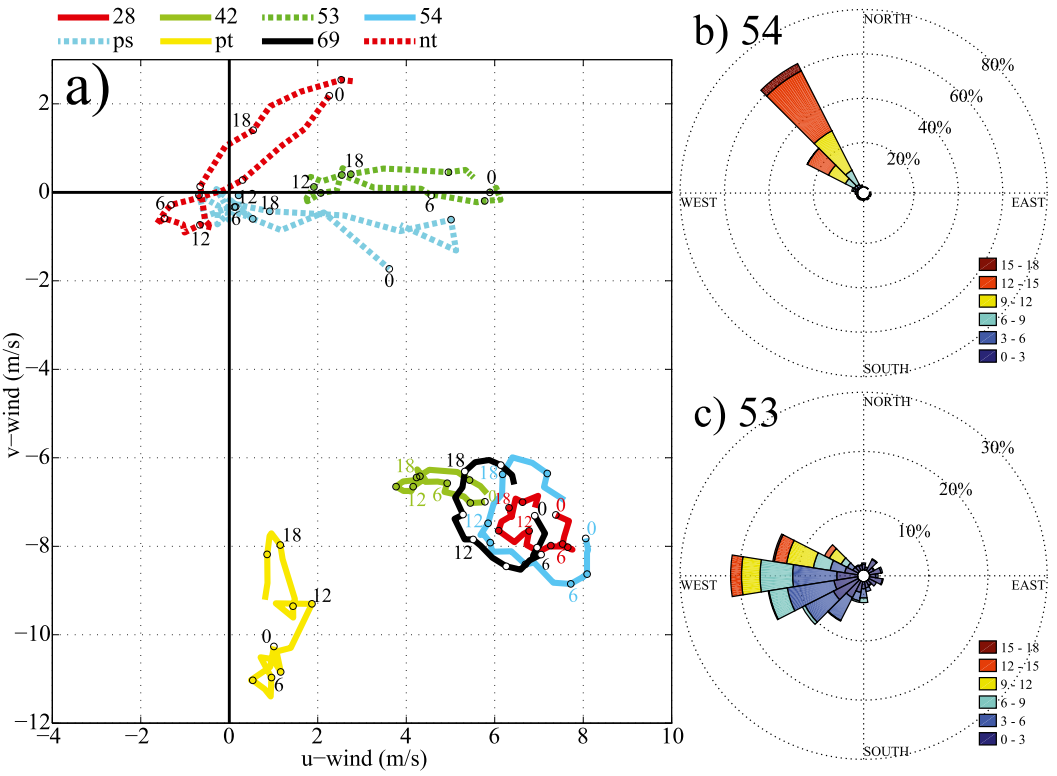

FIG. 2. (a) Temporal hodographs of the average diurnal cycle during PreAMBLE for buoy and coastal stations shown in Fig. 1b. Wind roses (m s^{-1}) during PreAMBLE are shown for buoys (b) 54 and (c) 53.

on these surface observations, but as will be demonstrated later with the aircraft observations, the atmosphere just above the surface is not necessarily well reflected by measurements at the surface.

c. *Lower atmospheric features during PreAMBLE*

At Vandenberg Air Force Base (VBG) weather balloons are launched daily at 1200 UTC. The wind direction in the lowest 2.5 km is generally out of the north-northwest (NNW) during PreAMBLE (Fig. 3). The exception is a strong northeasterly wind above 1.5 km that coincided with the initiation of a southerly surge that occurred on the last day of the project (Parish et al. 2015). Not surprisingly, the temperature profiles near the surface display little variability. A temperature inversion appears in the mean profile from about 250 to 1000 m. The base of the temperature inversion is used to identify the top of the MBL in each sounding similar to other MBL studies (e.g., de Szoeke et al. 2012). The upper and lower quartile of MBL heights are 285 and 560 m with a median of 420 m.

Since the VBG soundings only occur once a day, additional observations of the lower atmosphere were sought to characterize the variability of the lower atmosphere during PreAMBLE. Research flights give excellent, targeted measurements but lack continuous measurements needed for long-term monitoring of the lower atmosphere. To identify the diurnal cycle and synoptic influence on the MBL height near the California bight, Aircraft Meteorological Data Reports (AMDARs) from commercial aircraft arriving and departing Los Angeles International Airport (LAX) are used to provide a near-continuous depiction of the lower atmosphere (Fig. 4). Observations from AMDAR of wind, temperature, and the corresponding MBL heights were processed using the same methods described in Rahn and Mitchell (2016). Only profiles from aircraft to the west of LAX over the ocean that are taking off or landing are used (cf. Fig. 1a in Rahn and Mitchell). The coastline in vicinity of LAX is oriented NNW–SSE. Times with a sounding are indicated with black dots along the top of the plot. Temperature and wind are interpolated, but individual MBL height observations are not. Winds are only shown every 6 h for clarity.

The distance between LAX and PAPC is about 190 km, but any synoptic disturbance will impact both locations. Although synoptic-scale subsidence is normal over the region, the downward motion either relaxes or is replaced by upward motion during the passage of an upper-tropospheric trough. Weakening of the large-scale

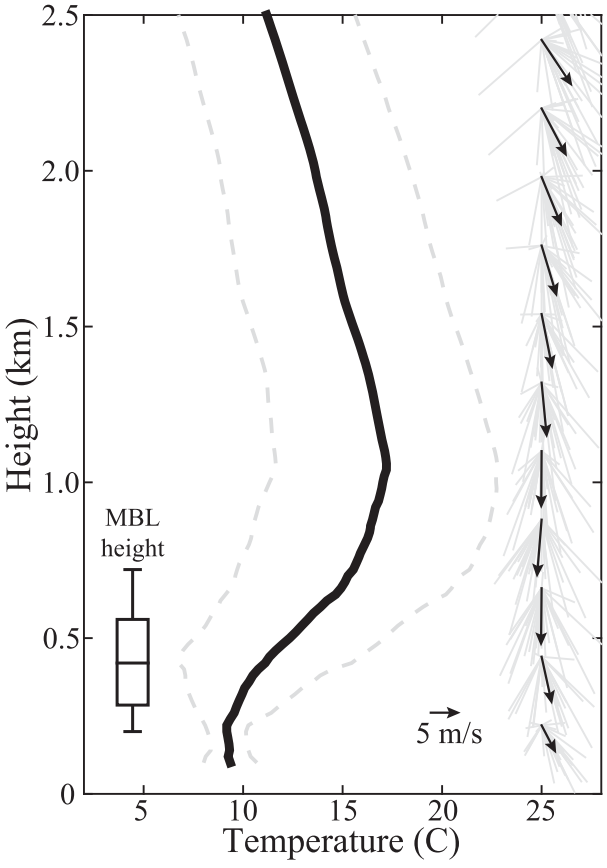

FIG. 3. From the 1200 UTC VBG soundings during PreAMBLE. Average temperature profile (°C, solid black) with one standard deviation (dashed gray), average wind vectors (m s^{-1}, bold vectors) with individual wind vectors (gray, headless vectors), and a boxplot of MBL height indicating the quartiles and whiskers extending to the 10th and 90th percentiles.

subsidence or more onshore wind corresponds to a deepening of the coastal MBL. The most obvious disturbance occurs after 24 May when the height of the MBL increases dramatically and is associated with a cold temperature anomaly. The cold temperature anomaly is associated with the passage of a deep upper-level trough (not shown). Two other weaker disturbances from the passage of a trough occurred on 18 May and 5 June and had a smaller response in the MBL height. Neglecting the larger perturbations to MBL heights during the passage of the three troughs, the depth of the MBL at LAX tended to be shallower in May and deeper in June.

The mean diurnal cycle of MBL height, potential temperature, and wind during PreAMBLE is depicted in Fig. 5. The mean diurnal cycle is constructed by taking all AMDAR observations during PreAMBLE, interpolating them to a regular height grid, and binning them hourly. Several features of the average diurnal cycle at LAX are important to the synthesis and explanation of the PreAMBLE measurements in the SBC. The greatest MBL height occurs at about 1600 UTC, which is a few hours after sunrise.[2] The increase of the MBL depth throughout the night and into the morning hours (0300–1600 UTC) is accompanied by an east wind directed toward the SBC within the MBL. Early morning satellite imagery during PreAMBLE frequently showed movement of the MBL cloud near LAX toward the SBC before stagnating and evaporating later in the day. Wind speed during the evening to morning hours tends to be greatest at the top of the MBL and decreases toward the lowest levels, which highlights the usefulness of the AMDAR data in providing information above the surface. If just surface features are used, the alongshore component at the surface is much less pronounced than that occurring at the top of the MBL, and it might be overlooked.

Above the MBL, the wind shifts from the northwest after sunset (0300 UTC) to northeast in the midmorning (1600 UTC). The wind shifts to the southwest when a well-developed sea breeze becomes established after 1800 UTC. A sharp decrease in the MBL height coincides with the onset of the sea breeze and the depth of the MBL increases again after sunset. Since all of the PreAMBLE flights take place from midmorning to late afternoon, it is the conditions that develop overnight and into the morning that set the stage for what is observed during the research flights.

3. Synthesis of PreAMBLE measurements

a. Flight strategies and previous case studies

Research flights (RFs) during PreAMBLE are summarized in Table 1, which includes the location, flight pattern, and objective of each mission. In total, 11 flights passed near PAPC, 3 flights examined a Catalina eddy, and 1 flight examined island wake effects in the lee of the Channel Islands. Several flight strategies were adopted to examine the flow around PAPC and include the spoke, triangle, ladder, and isobaric mapping pattern (Fig. 6). The aircraft either ascended and descended to obtain vertical profiles or flew at a constant pressure using the autopilot. The height is measured while the aircraft flies at a constant pressure and the slope of the isobaric surface is a measure of the horizontal pressure gradient force (PGF), and thus the forcing. While conceptually simple, in practice this method is difficult since

[2] On 1 June 2012, sunrise occurs at 1242 UTC and sunset occurs at 0306 UTC.

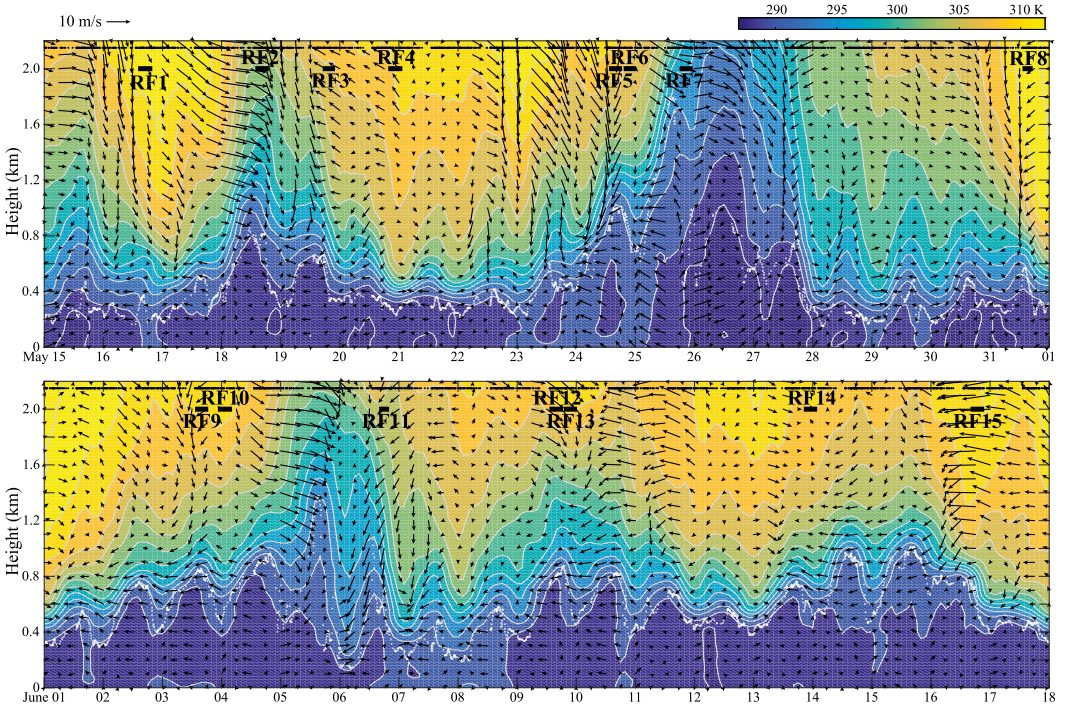

FIG. 4. Time series of AMDAR soundings at LAX depicting interpolated potential temperature (K, color scale), interpolated horizontal wind vectors (m s^{-1}) only shown every 6 h and 100 m with the scale in the upper left, and the MBL height from each sounding (white dots). Times of each research flight are indicated by the thick black lines at 2 km.

the small slope of the isobaric surface requires precise measurements. For example, a 10 m s^{-1} geostrophic wind at 43° latitude corresponds to an isobaric slope of 10^{-4}, which represents a vertical change of 1 m over a horizontal distance of 10 km. Precise height measurements are obtained using differential GPS processing. Small deviations of the aircraft from the selected pressure level can easily be compensated for by a hydrostatic

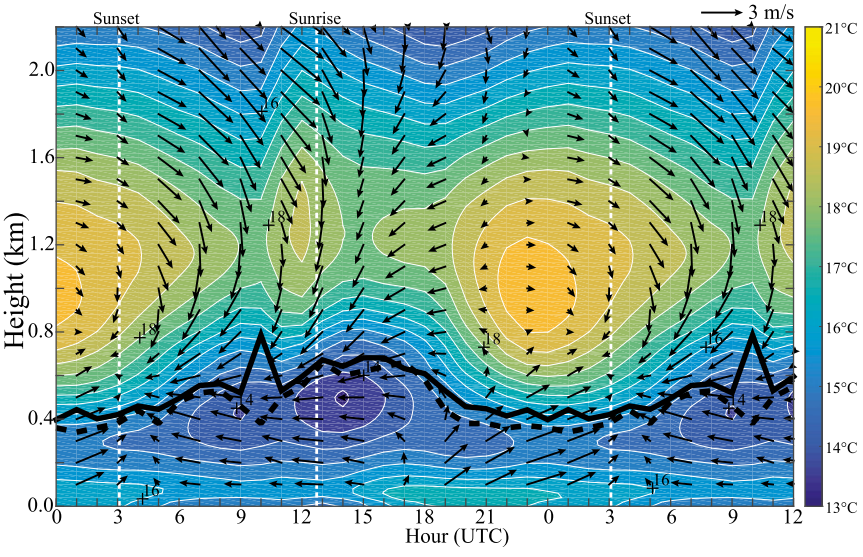

FIG. 5. Average diurnal cycle (0000–1200 h repeated) using hourly bins at LAX from AMDAR during PreAMBLE of horizontal wind vectors (m s^{-1}, scale at upper right), temperature (°C, color fill and contoured every 0.5°C), and the average and median MBL height are represented by the solid and dashed black lines, respectively.

TABLE 1. Summary of flights including location [Santa Barbara Channel (SBC), Point Conception (PC), Point Buchon (PB), Catalina Island (CAT), Channel Islands (CIs), and Monterey Bay (MRY)], flight pattern, and mission objective.

Flight	Date	Takeoff (UTC)	Location	Flight pattern	Objective
RF01	16 May	1432	SBC, PC	Isobaric mapping	Horizontal pressure field within SBC and north of PC
RF02	18 May	1433	SBC, PC	Isobaric mapping	Horizontal pressure field within SBC and north of PC
RF03	19 May	1752	SBC, PC	Triangle	Isobaric and vertical profiles around PC
RF04	20 May	2030	SBC, PC	Ladder	Detailed isobaric mapping of pressure field near PC
RF05	24a May	1404	SBC, coast to MRY	Profiling/isobaric	Low-level structure upwind of PC/near PB
RF06	24b May	2002	SBC, PC	Spoke	Adjustment of wind and pressure west of SBC
RF07	25 May	1850	SBC, PC	Spoke	Adjustment of wind and pressure west of SBC
RF08	31 May	1356	CAT	Eddy	MBL height and isobaric pressure field of Catalina eddy
RF09	3a Jun	1401	SBC, PC	Triangle	Isobaric and vertical profiles around PC
RF10	3b Jun	2020	SBC, PC	Spoke	Adjustment of wind and pressure west of SBC
RF11	6 Jun	1647	CAT	Eddy	MBL height and isobaric pressure field of Catalina eddy
RF12	9a Jun	1354	CAT	Eddy	MBL height and isobaric pressure field of Catalina eddy
RF13	9b Jun	1949	CIs	Ladder	Topographic influence of CIs on wind and pressure
RF14	13 Jun	2110	SBC, PC, PB	Profiling/isobaric	Eddy circulation in SBC, low-level structure north of PC to PB
RF15	16 Jun	1653	SBC, PC	Spoke	Initiation of southerly surge north of PC

correction using in situ pressure and temperature measurements (Parish et al. 2007).

During the spoke pattern the aircraft repeatedly flew through the same point at the center of the spoke, allowing any pressure tendency to be obtained and used to correct isobaric surfaces during the flights. The triangle pattern is centered more on the headland with legs orientated at 45° or 90° to each other. The isobaric mapping covers a broad area to obtain the distribution of heights on the pressure surface from north of PAPC into the SBC. The ladder pattern is a compact set of legs designed to map the isobaric height distribution over a fine spatial area near the transition into an expansion fan. Patterns typically included a combination of soundings between about 150 and 900 m and isobaric legs flown at a level of about 990 hPa. One of the four patterns in Fig. 6 was used in 10 out of the 15 research flights.

One goal is to find common aspects of the flow for all of the flights in vicinity of PAPC and the SBC that may be considered typical for this location and time of year. The response of the coastal flow to the dramatic change of the coastline near PAPC was highlighted in several papers. Rahn et al. (2013; RF03) used the precise measurements to compare the actual atmospheric response to what would be expected under an idealized scenario (channel flow analogy and Bernoulli's equation for inviscid flow), which explained most of the response. Differences were attributed to factors such as the change of inversion layer thickness or thermal gradients above

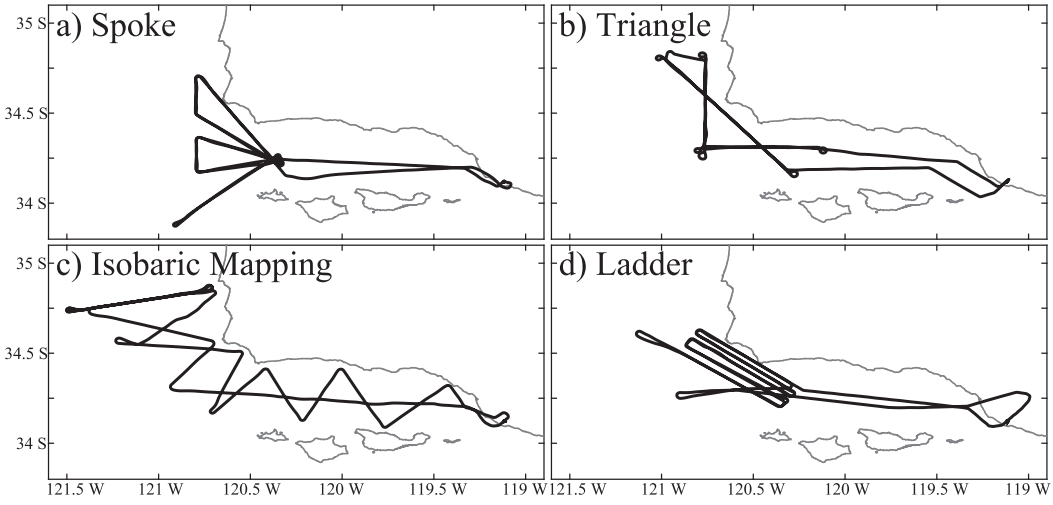

FIG. 6. Primary flight patterns for investigating transition around Point Conception.

the MBL. Parish et al. (2014; RF04) presented a case where the transition was strongly influenced by offshore flow. Rahn et al. (2014; RF10) revealed how easterly flow in the SBC interacted with strong northwesterly flow from north of Point Conception. Parish et al. (2016a; RF14) modeled the expansion fan and used D-value cross sections from the aircraft and simulation to assess the vertical profile of the horizontal PGF. D-values are the deviations of actual height above sea level from the *U.S. Standard Atmosphere*, *1976* table (COESA 1976), which effectively removes the vertical component of the PGF, thereby allowing direct visualization of the horizontal PGF (Parish et al. 2016b).

Several missions captured other phenomena besides the expansion fan transition and used flight strategies different than in Fig. 6. Near Point Buchon on 24 May 2012, which was a particularly windy day, Rahn et al. (2016; RF05) found evidence that Kelvin–Helmholtz instability was responsible for creating a secondary well-mixed layer above the MBL. Of the three Catalina eddy flights, two eddies dissipated rapidly at the beginning of the missions, leaving little measureable signal. One flight captured a well-developed Catalina eddy (Parish et al. 2013; RF12) and revealed that blocking of the onshore flow south of Los Angeles enhanced the MBL height and was associated with a locally high pressure at the coast. Northward flow on the eastern edge of the cyclonic circulation was supported by the horizontal pressure field and little evidence of leeside troughing south of Santa Barbara was observed. Parish et al. (2015; RF15) examined the onset of a southerly surge and found that southerly ageostrophic winds associated with higher pressure in the south supported the northward movement of the marine stratus. Offshore flow of warm, continental air was observed north of Point Arguello and altered the pressure field adjacent to the coast.

b. *Transition into expansion fan*

Eight of the flights that occurred near PAPC included at least one isobaric leg along a roughly northwest axis meant to capture the transition of the flow around the headlands (Fig. 7a). The flight tracks are not all along the exact same path, so a common reference point of 34.9°N, 120.95°W is used to calculate the horizontal distance for each isobaric leg. Isobaric height measurements during the eight different flights reveal the diversity of how the flow transitions around PAPC. All of these flights occur from midmorning to late afternoon and represent moderate to strong coastal jet cases where the isobaric height decreases toward the southeast. The exception is RF15 that occurred during the initiation of a southerly surge where the isobaric height decreases toward the northwest instead. To get a sense of the strength of the PGF directed along the leg, several slopes and their associated cross-leg geostrophic wind at 34.5°N are provided in the upper right of Fig. 7b. Isobaric surfaces are clearly not linear over the entire flightpath, but the corresponding cross-leg geostrophic wind varies between 10 and 40 m s^{-1}.

Changes to the slope of the isobaric surface within the MBL represent not only changes to the PGF but also reflect changes to the MBL depth that are associated with hydraulic features. For instance, RF03 shows a relatively clean signal of a compression bulge centered around 35 km that transitions into the expansion fan farther to the south. RF09 and RF10 have a downward slope only in the northwestern half of the leg and in the southeastern half the isobaric surface either becomes flat or is sloped slightly down toward the northwest. RF09 and RF10 occurred on 3 June when there was a layer of easterly flow between the MBL below and the free troposphere above. The weakest PGF was observed during RF07, but the isobaric surface still showed some evidence of a compression bulge that transitioned into an expansion fan. RF15 was the last flight of the project and captured the initiation of a southerly surge out of the California bight. It was the only flight where the isobaric surface sloped down toward the northwest.

Many flights exhibit distinct wavelike features in the expansion fan with different amplitude and wavelengths. A single anomaly is embedded in the expansion fan in RF03 and RF04. Multiple, high-amplitude waves are present in the steeply sloped expansion fan observed during RF05 and RF06, which were both flown on the strongest wind day of 24 May. The wave during RF06 is much broader than other flights. We speculate that these waves are tied to topographic waves, but a direct connection was not observed since flying over the land near Vandenberg Air Force Base was not possible. Table 2 lists the 1.5-km wind from the 1200 UTC sounding at VBG for each flight in Fig. 7. Although the evidence is inconclusive, the soundings suggest that there may be some relation to the cross-barrier flow. The most prominent wave features in the isobaric legs during RF05 and RF06 occur when there is a 15 m s^{-1} wind from the north, which is the strongest among these flights. The 1.5-km wind at VBG during RF03, RF04, RF09, and RF10 was also out of the north, but with weaker speeds of 7–10 m s^{-1}. RF03 and RF04 had only one spike in the isobaric height and their amplitude was less than that seen in RF05 and RF06.

Little indication of wave activity appears in RF09 and RF10, but this could be due to the influence of the layer that extends to about 500 m that contains easterly wind (see Fig. 10). During RF07 the wind speed over VBG at

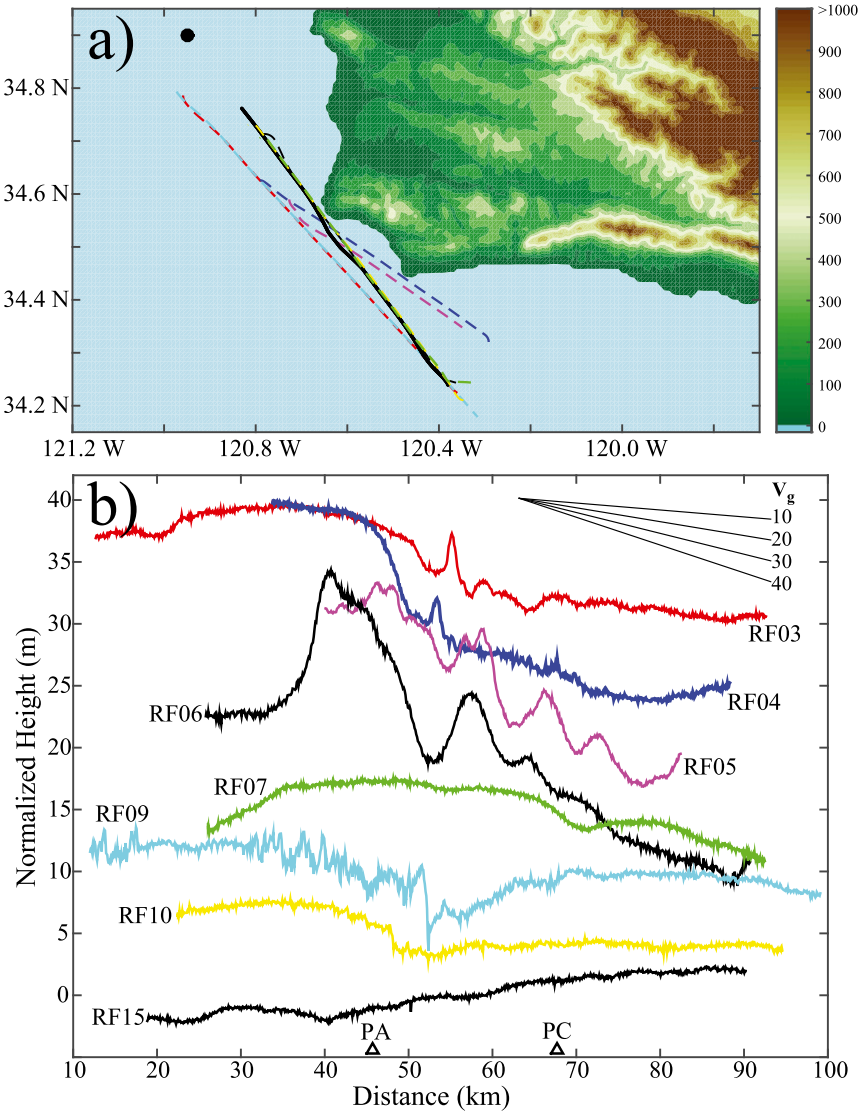

FIG. 7. (a) Topography (m, color bar) and flight tracks of one NW–SE isobaric leg per research flight. The large black dot is the common point of 34.9°N, 120.95°W that is used to calculate a common horizontal distance. (b) Isobaric height during the legs with the mean of each leg removed and offset by 5 m for each flight. In the upper right of (b) are slopes and their corresponding geostrophic wind (m s^{-1}). Locations of PA and PC are indicated with triangles.

1.5 km is 13 m s^{-1}, but unlike all of the other flights the direction is from the northwest and there is little evidence of any substantial wave activity in the height of the isobaric surface. Even though the flow within the MBL during RF07 is similar to other flights, the slope near PAPC during RF07 is much less than other flights. The major difference is the lack of cross-barrier flow aloft, which points to how the underlying hydraulic features such as an expansion fan can be modified by external processes. Thus, the comparison of all flights that had an isobaric leg near PAPC helps substantiate the role of offshore flow in modifying the transition around PAPC as described for the RF04 case in Parish et al. (2014).

On board the aircraft were upward- and downward-pointing Wyoming Cloud lidars (WCLs) that provide a two-dimensional depiction of the transition near PAPC (Fig. 8). The WCLs are a pair of 355-nm lidars designed for retrieval of cloud and aerosol properties and details of the WCLs can be found in Wang et al. (2009) and Wang et al. (2012). Here, the primary role of the WCLs is to detect sharp gradients in attenuated backscatter and linear depolarization ratio that are used to identify layering in the atmosphere. The top of the well-mixed

TABLE 2. Wind speed ($m\,s^{-1}$) and direction (°) interpolated to 1.5 km from the 1200 UTC sounding at VBG for each flight depicted in Fig. 7.

Flight	Speed	Direction
RF03	10	5°
RF04	7	0°
RF05/06	15	2°
RF07	13	315°
RF09/10	10	353°

MBL underneath the free troposphere is easy to detect in the lidar returns but more subtle layering is also evident.

Features from the isobaric heights in Fig. 7, which are related to the depth of the MBL, also appear in the lidar cross sections. Depth of the MBL upwind of PAPC is 200–400 m with heights closer to 400 m in the compression bulge, which is near the median of MBL height detected from the soundings at VBG (Fig. 3). MBL depth in the expansion fan reaches ~100 m for most cases. The only lidar image that shows unambiguous layering above the expansion fan is RF10, which was due to easterly winds in the SBC that reached PAPC (Rahn et al. 2014). As a first-order approximation, the transition around PAPC conforms to the hydraulic response of a transcritical or supercritical two-layer shallow-water system bounded by a lateral boundary that turns away from the flow, which could be modified by external features. The numerous observations reveal that the response farther east into the SBC, however, is more complicated.

c. *Soundings in SBC*

Most flight time was spent in the vicinity of PAPC, but many observations were obtained in the SBC during the ferry out of and back to Point Mugu. The common flight pattern consisted of a series of ascents and descents along a constant zonal heading. Individual soundings and lidar images reveal the complex nature of the lower atmosphere in the SBC, but the discussion will begin with a representation of the mean conditions in the SBC. An average zonal cross section is created from all 90 vertical profiles (individual ascents and descents) taken within the SBC (Fig. 9a). Observations are linearly interpolated onto a regular grid and smoothed. Even with 90 individual soundings, there are sampling issues with constructing the mean cross section. Most samples are taken in the midmorning to late afternoon when there was a moderate to strong coastal jet near PAPC. On days with a prominent Catalina eddy, the aircraft sampled south of Point Mugu and did not enter the SBC. As a result, the composite best represents the lower atmosphere from midmorning to late afternoon during a moderate to strong coastal jet near PAPC. Although there are issues due to interpolation and the inconsistent spatial and temporal sampling, the composites point to several dominant features.

At the lower western edge of the composite, the cool MBL and strong northwesterly flow originating from north of PAPC is clear and the isentropes slope downward toward the east. The wind is weaker and westerly below 200 m and farther to the east. At upper levels there is warm, dry air associated with the subsiding air from the continent since the wind is primarily from the east-northeast. In the 200–600-m layer east of 120.2°W, there is an area of weak wind and moderate temperatures with little vertical gradient, and the mixing ratio is relatively high compared to the rest of the composite and increases toward the east. As seen in RF10 (Rahn et al. 2014), there is some evidence of a shallow (<200 m) cold MBL with a west wind, a much warmer free troposphere above ~800 m, and a cool, relatively moist layer with light wind on average that is in between the shallow layer and free troposphere above.

The composite resembles a more diffuse version of the lower atmosphere observed during RF10. To see if there is a similar structure in the SBC on other days, individual profiles of temperature and wind vectors from eight research flights are plotted in Fig. 10. A weak low-level inversion underneath a more intense upper inversion was measured on 6 days over 8 flights. Between the two inversions is a layer that exhibits a lapse rate that ranges between nearly isothermal (RF06) to dry adiabatic (RF10). The wind profile alone can indicate distinct layers, such as during RF02, RF03, and RF09. At other times the wind profile does not clearly demark distinct layers, which is perhaps due to the aircraft not penetrating low enough into the shallow MBL or high enough into the free troposphere. The inversion at the lowest layer tends to be shallow such that the in situ measurements just reach the top of this lowest layer.

To supplement the in situ data that may not reach the shallow MBL near the surface, the WCLs can detect the layering that exists within the SBC (Fig. 11). The signal in the lidar returns can be somewhat subtle or disorganized, but the main features can be discerned. For instance, in RF02 there is a continuous decrease of the MBL from the western edge down toward the surface around 1730 UTC. Above that thinning layer into the SBC is a more disorganized layer above, but it is associated with the deeper well-mixed layer that is capped by a strong inversion as seen at the top of the soundings in Fig. 10. In RF10 there are clouds at the top of the well-mixed SBC layer, which slopes down from east to west. Underneath is a shallow MBL that is slightly cooler as indicated in the sounding in Fig. 10. The lowest layer in

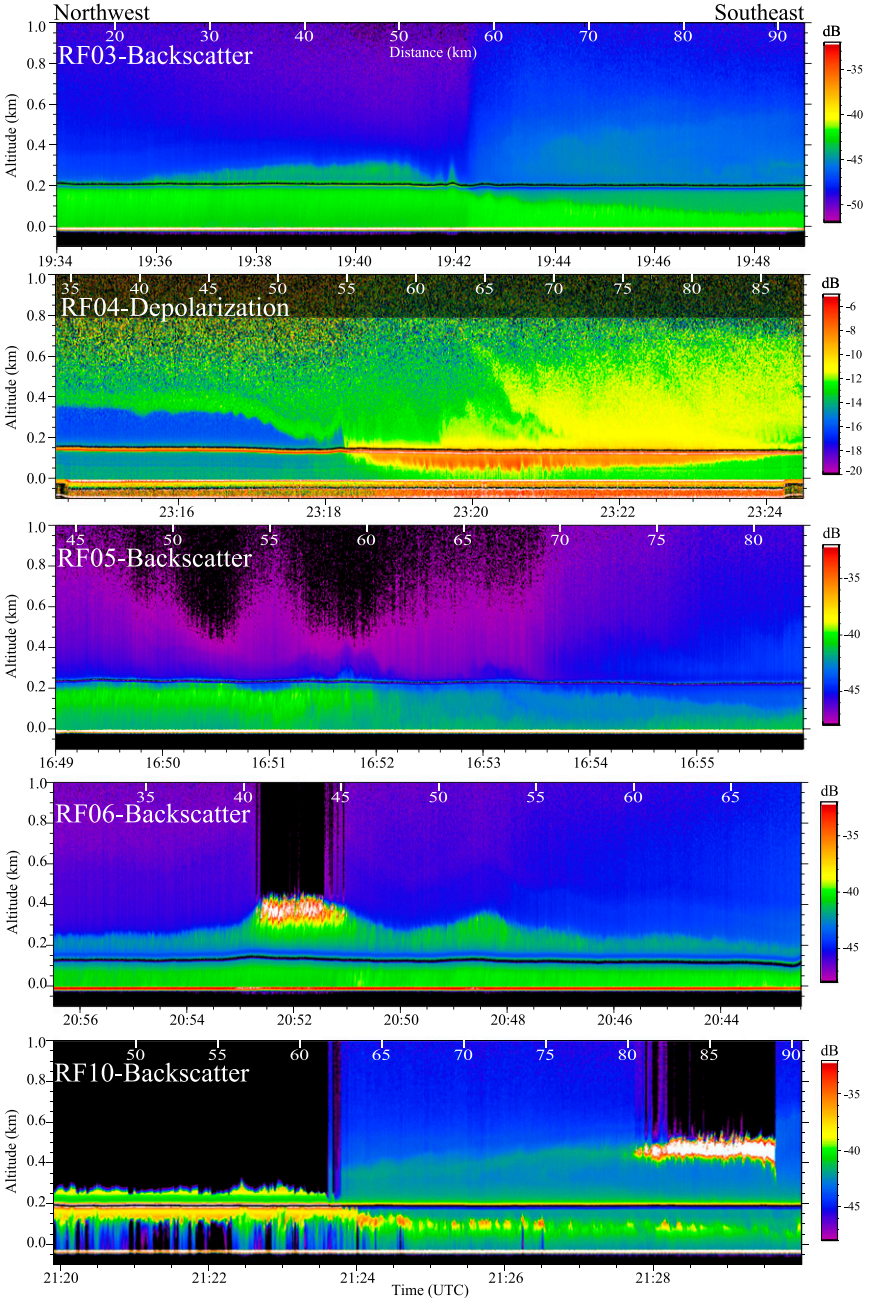

FIG. 8. Lidar returns of uncalibrated attenuated backscatter or depolarization ratio (dB) for PAPC tracks during the research flights indicated in the upper left of each panel with northwest to the left and southeast to the right. The distance from the common point shown in Fig. 7a is indicated at the top of each panel. Horizontal lines near 200 m indicate the flight tracks.

the west can be traced back to the MBL accompanying the northwesterly flow rounding PAPC.

The notable exception occurred during RF06 when a fairly robust signal of the MBL top was detected (Fig. 11). A strong vertical gradient in backscatter suggests a strong inversion layer that inhibits entrainment and mixing into the shallow MBL. The westernmost sounding in RF06 (not shown) indicated a temperature inversion of 8°C at the top of the lowest layer. More detail of this specific case can be found in Juliano et al. (2017, manuscript submitted to *J. Appl. Meteor. Climatol.*). Between 2033 and 2034 UTC there is a signal that strongly suggests that a hydraulic jump has formed where the shallow MBL rises sharply. No other flight detected a hydraulic jump.

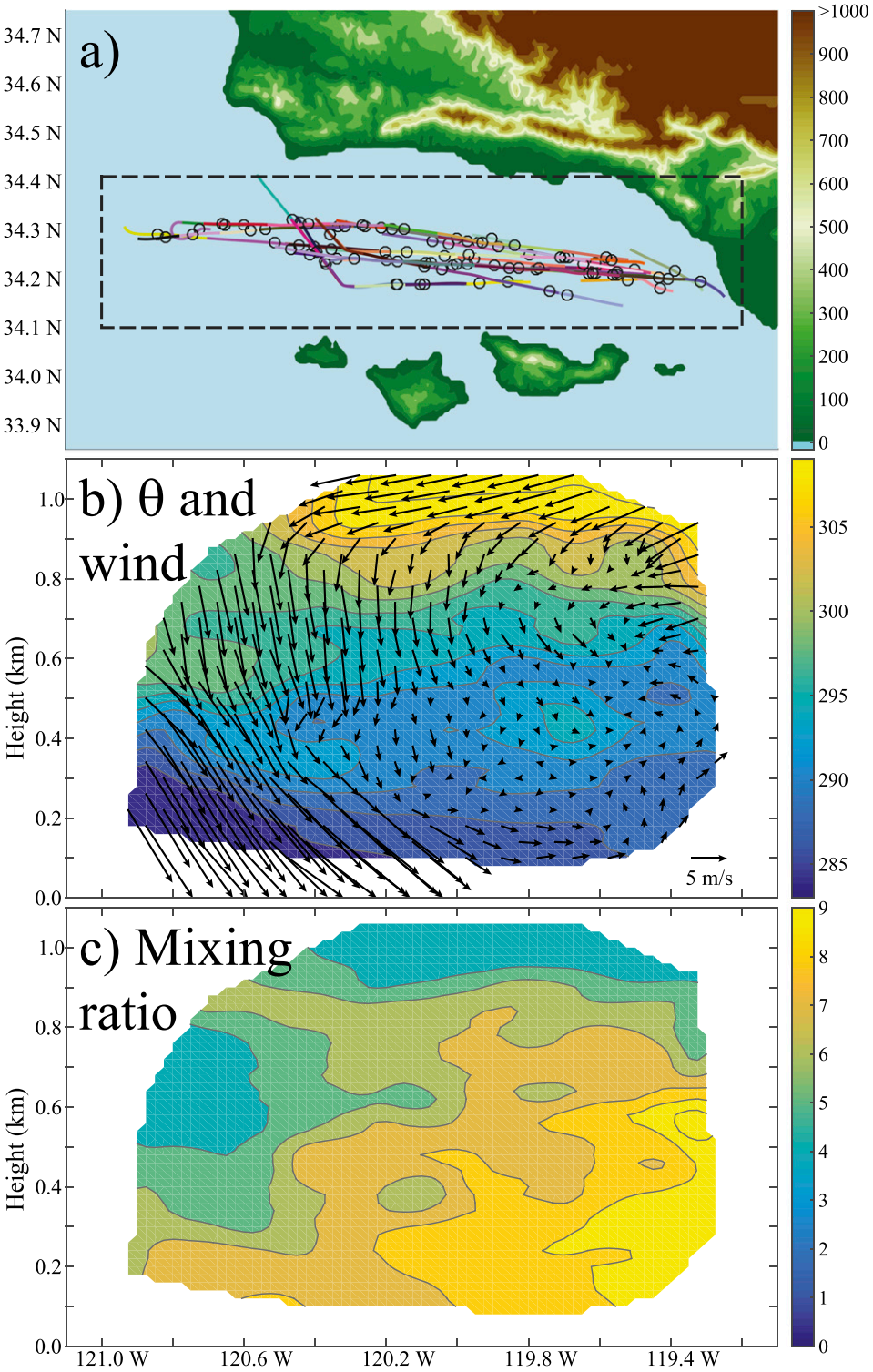

FIG. 9. (a) Topography (m, color bar) and the flightpaths that comprise all 90 soundings in the SBC as defined by the dashed box. Circles represent where the aircraft passed through an inversion. Composites of (b) potential temperature (K, color bar) and horizontal wind vectors and (c) mixing ratio ($g\,kg^{-1}$, color bar).

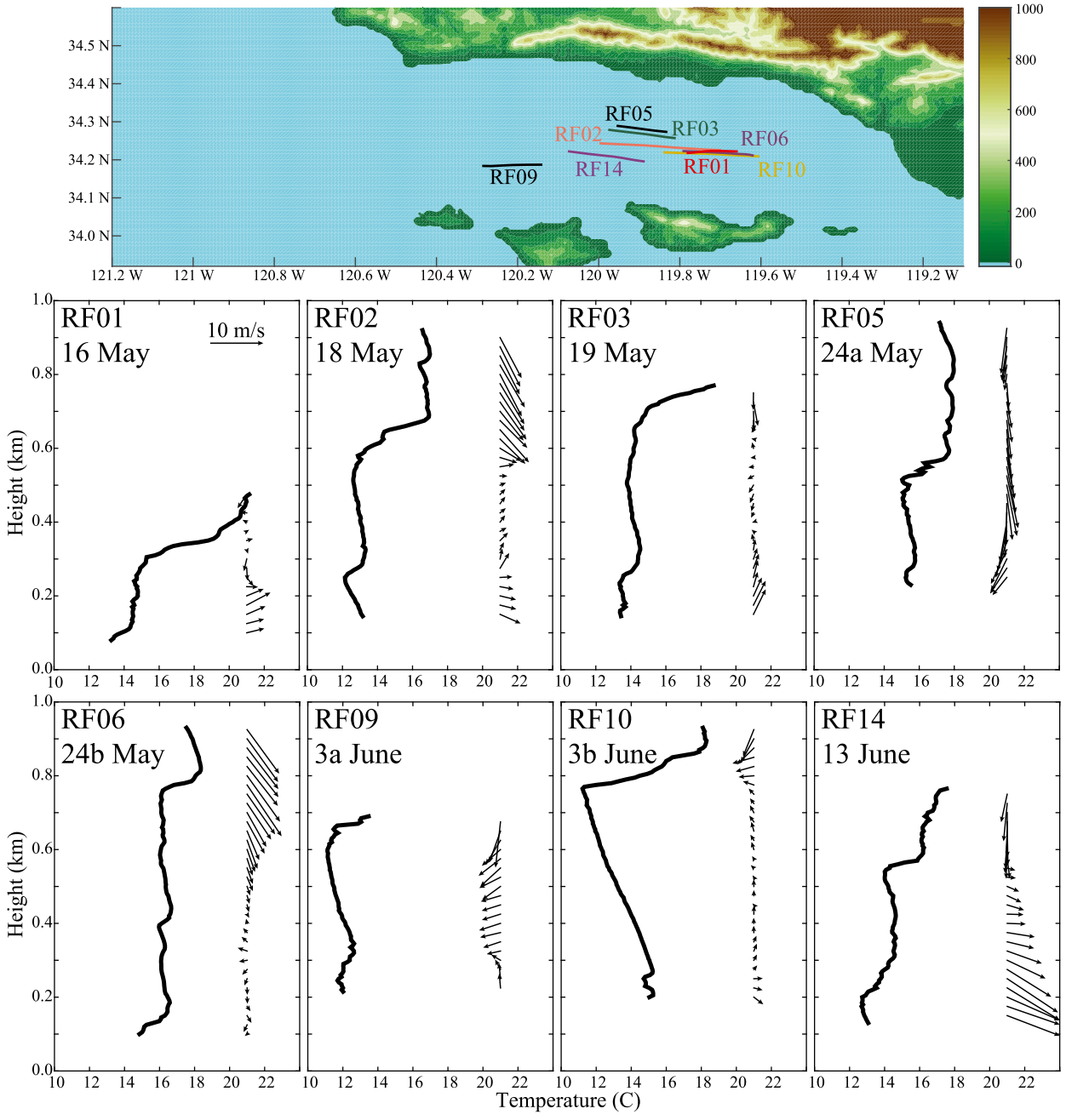

FIG. 10. Example soundings of temperature (°C) and wind (m s^{-1}, scale in the RF01 panel) within the SBC.

The hydraulic jump nearly reaches 200 m, but the aircraft did not sample this layer in situ. East of the hydraulic jump, the single sharp vertical gradient in the backscatter weakens. The RF06 sounding in Fig. 10 is located in the eastern part of the SBC and detects the top of an inversion just below 200 m and another inversion layer near 800 m, which is associated with an increase of wind speed from the northwest. There is weak wind from the east in the 200–400-m layer.

Modification of the near-surface air during RF09 was particularly pronounced and it is used to highlight key processes occurring as the low-level flow enters the SBC (Fig. 12). Most of the triangle pattern flown in RF09 was cloudy with a small break in cloud above the expansion fan. Similar to many flights, the MBL depth increased in a compression bulge just upstream of PAPC and rapidly thinned into the expansion fan. The steep MBL collapse is in part due to the east wind found over the

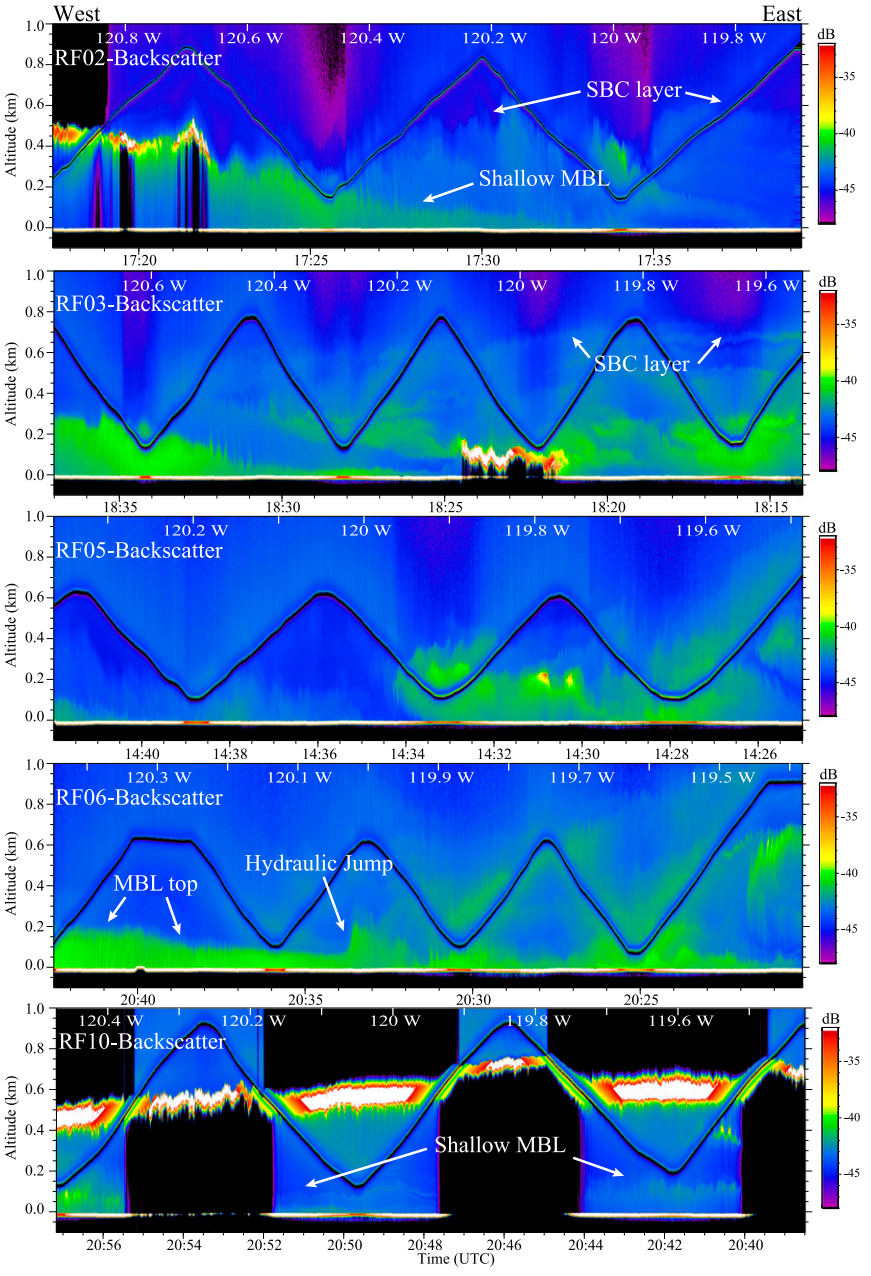

FIG. 11. Lidar returns of uncalibrated attenuated backscatter (dB) for SBC tracks during the research flights indicated in the upper left of each panel with west to the left and east to the right.

SBC that encounters the northwest wind found near PAPC. The sounding closest to buoy 54 (Fig. 12a) indicates easterly wind from about 250 to 500 m. The aircraft does not penetrate deep into the shallow layer, but below 250 m the temperature and dewpoint decrease and the wind is out of the northwest, which is similar to conditions in the MBL upstream of PAPC. Although the temperature and dewpoint at the top of the profile are perturbed by turbulent motion (inferred from large perturbations in the profile and high eddy dissipation rate, not shown), the warm and dry free troposphere begins around 500 m.

The key feature of this profile is the temperature difference in the layers, which represents the history of air parcels at each level. Although the aircraft does not measure temperature just above the surface, three nearby buoys provide the necessary information. Air temperature is measured at a height of 4 m and the water

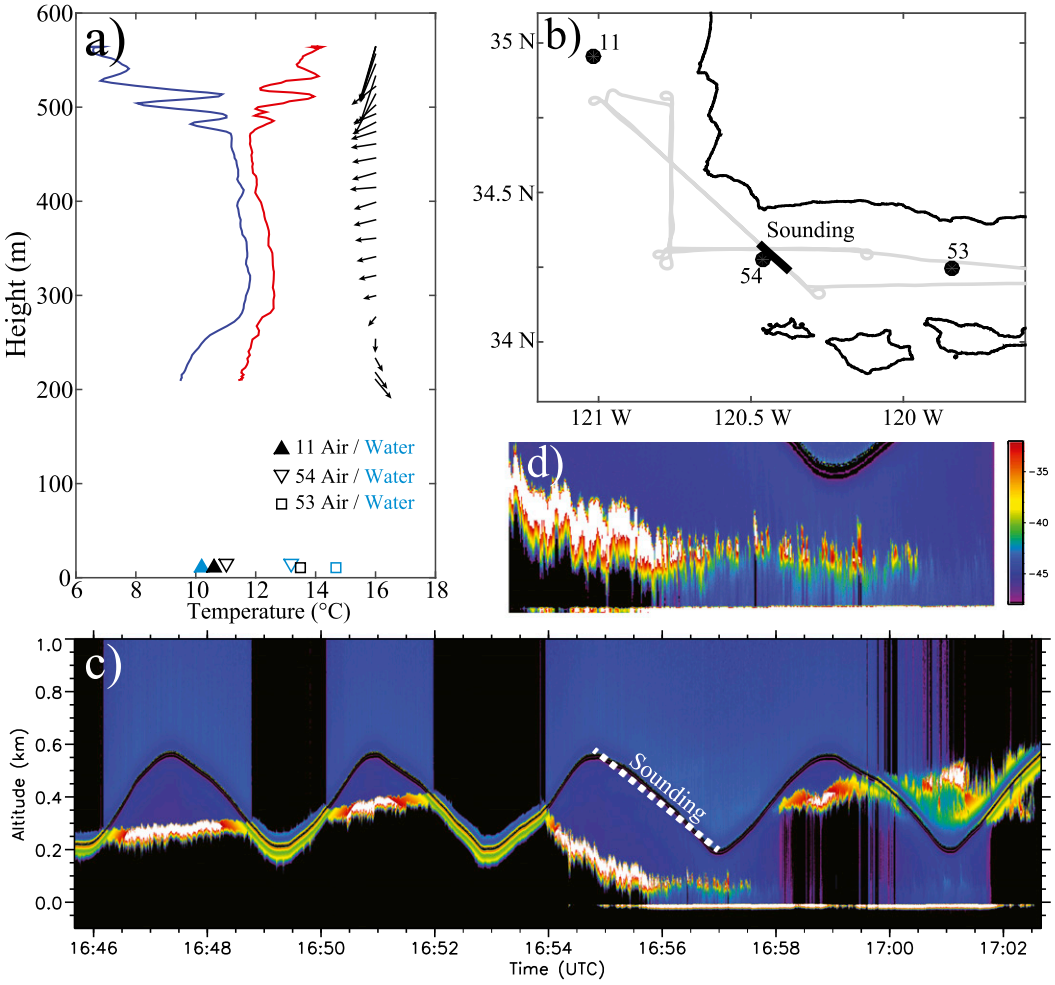

FIG. 12. (a) Profile of temperature (°C, red), dewpoint temperature (°C, blue), and wind (m s^{-1}, vectors). Symbols at the bottom of the panel indicate the air (black) and water (blue) temperature (°C) at buoys 11 (closed triangle), 54 (open triangle), and 53 (square). (b) Location of buoys (filled circles) and flight track during RF09 (gray) with the sounding indicated by the black portion of the flight track. (c) Copolarized power (dB) from upward- and downward-pointing WCL along the NW–SE leg near PAPC with the sounding indicated by the dotted white line. (d) A detail of (c) from 1655 to 1658 UTC.

temperature is measured at a depth of 0.6 m. Since the sounding near buoy 54 was taken around 1656 UTC, the 1700 UTC buoy observations are used. North of PAPC at buoy 11 the air and water temperature are similar with temperatures of 10.6° and 10.2°C, respectively. Just south of Point Conception at buoy 54, the water temperature has increased to 13.2°C, but the air temperature has only increased to 11.0°C.

As the cool air passes over the warmer water with a 4-m wind speed of 9.2 m s^{-1} at buoy 54, the air must warm through sensible heat flux since the water is 2.2°C warmer than the air. Convection will mix and warm the lowest layer as it enters the SBC. Backscatter from the WCL near buoy 54 clearly displays the convective nature because of the distinct plumes of higher backscatter near the surface (Fig. 12d). Farther east toward buoy 53, the air and water temperature both increase and the lowest layer, while still discernable, has lost its sharp features. The transition of the near-surface flow around PAPC is presented in a Lagrangian sense, which is supported in part by previous modeling efforts that indicate streamlines passing near the three buoys [cf. Fig. 9 in Parish et al. (2016a)]. The near-surface air is modified as it transitions from the cool, upwelled waters north of PAPC toward the warmer sea surface temperatures that exist in the SBC (Fig. 1b). In fact, during PreAMBLE at buoys 11, 54, and 53, respectively, the average air temperature was 11.3°, 12.0°, and 14.1°C and the average difference between the water temperature and air temperature ($T_{water} - T_{air}$) was −0.3°, 1.0°, and 0.4°C. These

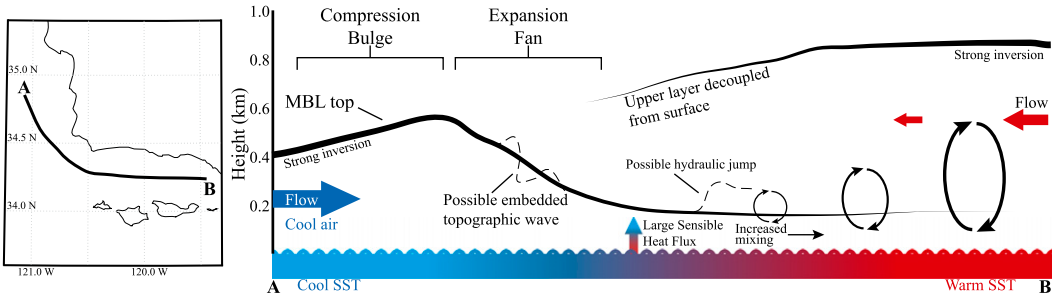

FIG. 13. Conceptual model of the typical midmorning to late afternoon vertical structure during a moderate to strong coastal jet.

differences are all significantly different than zero at the 99% confidence level using the bootstrap method and randomly resampling 10 000 times to construct the frequency distribution.

4. Conclusions

A conceptual model of the most common structure and principal processes in the SBC that occur from midmorning to late afternoon during PreAMBLE when the coastal jet is moderate to strong is presented in Fig. 13. The well-mixed MBL northwest of PAPC is fairly cool since the SSTs are typically much lower along the coast north of PAPC than they are within the California bight (Fig. 1b). A typical compression bulge and expansion fan occur near PAPC. Soundings at VBG (Fig. 3) suggest that stronger cross-shore (northerly) winds aloft might be tied to topographic waves embedded in the expansion fan, although no flights were able to pass over the land to verify this. The AMDAR diurnal cycle at LAX (Fig. 5) indicates that the flow is on average directed toward the SBC over a well-mixed, deep layer overnight and into the morning from 0600 to 1700 UTC with the greatest wind speed near the top of the MBL. During the morning the MBL cloud near LAX was often observed to be moving into the SBC in the visible satellite images before stagnating and evaporating later in the day. Offshore of LAX the SST is on average 4.5°C warmer than offshore of PAPC (Fig. 1b) and the average MBL depth at 1600 UTC is 625 m near LAX. Many of the ~3-h research flights begin between 1400 and 2000 UTC when there is still easterly wind near the top of the MBL at LAX. Although not all soundings taken in the SBC (Fig. 10) show an east wind, the wind in the middle of the sounding (~200–600 m) is generally light. Some flights such as RF03 (Fig. 10) reveal easterly wind, but even on days with little advection, the warmer SST in the eastern part of the SBC would promote a relatively warm and deep layer compared to air originating from near PAPC.

When the northerly flow upstream of PAPC transitions into the expansion fan and encounters the relatively warm layer in the SBC, the cooler and denser air is confined to the lowest layer as it enters the SBC. The initially sharp contrast between the shallow MBL associated with the expansion fan and the warmer layer in the SBC weakens toward the east. Sensible heating of the cool air by the warmer SST promotes mixing and warming as the air enters into the SBC (Fig. 12d). Thus, the inversion separating the bottom two layers is eroded. The one notable exception is during RF06 when there was a strong inversion separating the two layers that inhibited vertical mixing. Strong layer separation is more conducive to hydraulic features that depend on sharp density contrasts between layers. During that flight, a distinct hydraulic jump developed, but farther east the signal in the backscatter was eroded, likely due to the addition of mechanically generated turbulence in the wake of the hydraulic jump.

The interface between the middle layer in the SBC and the free troposphere above is well defined in the east. Even though the middle layer may not be entirely well mixed and have uniform properties, there is typically a distinct transition into the free troposphere marking the top of the layer. Evidence of the middle layer is found in many of the soundings within the SBC (Fig. 10) and inferred from the lidar returns (Fig. 11). It should be noted that even though the top is usually well defined, some in situ profiles and most of the lidar images indicate nonuniform features contained within this middle layer that lead to a more complicated signal. Toward the west, the middle layer is decoupled from the surface by the cooler layer near the surface associated with the expansion fan (Figs. 7 and 8).

Details of the magnitude and height of the upper and lower inversion in the SBC, the extent of the east wind into the SBC, the presence of waves in the expansion fan, and so on vary from case to case. Characteristics toward the east end of the SBC depend on what occurred overnight farther to the south in the California

bight. Day-to-day variability of the lower atmosphere in the bight was revealed by AMDAR observations at LAX (Fig. 4). For example, an upper-level trough was approaching the region prior to RF09 and RF10 and the MBL during this time was deeper than average and included an easterly wind that was also stronger than average. Thus, the deep and cloudy MBL was well defined in the lidar images near PAPC. Even under this deep and cloudy layer there is still evidence of a shallow layer extending from the surface to about 150 m that is associated with flow north of PAPC (Fig. 12c).

One of the main new findings of this synthesis is that during PreAMBLE there was never a continuous transition of the MBL from north of PAPC to the eastern side of SBC (cf. Fig. 7 in Dorman and Koračin 2008) and that hydraulic jumps were rare. Since the fast, shallow flow from PAPC would eventually encounter slower, deeper flow in the SBC, a hydraulic jump was expected where the flow transitions from supercritical to subcritical. However, the observations indicate that the shallow water analogy often fails because mixing erodes the interface between the MBL and SBC layers so that the lower layer often dissipates before realizing a hydraulic jump. This will not occur in ideal two-layer systems such as water and air that do not mix due to their great density difference. The one day a hydraulic jump was detected happened when the inversion was particularly strong and the two-layer system held long enough to realize the hydraulic jump.

We propose that typically there are two distinct layers that overlap within the SBC. The lowest layer, which is associated with the cool air from north of PAPC, erodes toward the eastern end of the SBC. The upper layer, associated with warmer air from the California bight, erodes at the western end of the SBC where it is decoupled from the surface. In some cases, if the east wind is strong enough, a sharp boundary exists where the easterly wind from the SBC meets the northwesterly wind in the expansion fan. In the transition region both layers are present with varying degrees of strength. Previous conceptual models were inhibited by a lack of observations directly over the SBC, which data obtained during PreAMBLE have now been able to supplement.

Acknowledgments. This research was supported by the National Science Foundation through Grants AGS-1439515 and AGS-1439594. The field project was supported by AGS-1034862. The authors wish to thank pilots Ahmad Bandini and Brett Wadsworth, and scientists Jeff French and Larry Oolman for help with the PreAMBLE field study and UWKA measurements.

REFERENCES

Beardsley, R. C., C. E. Dorman, C. A. Friehe, L. K. Rosenfield, and C. D. Wyant, 1987: Local atmospheric forcing during the Coastal Ocean Dynamics Experiment 1: A description of the marine boundary layer and atmospheric conditions over a northern California upwelling region. *J. Geophys. Res.*, **92**, 1467–1488, doi:10.1029/JC092iC02p01467.

Burk, S. D., and W. T. Thompson, 1996: The summertime low-level jet and marine boundary layer structure along the California coast. *Mon. Wea. Rev.*, **124**, 668–686, doi:10.1175/1520-0493(1996)124<0668:TSLLJA>2.0.CO;2.

——, T. Haack, and R. M. Samelson, 1999: Mesoscale simulation of supercritical, subcritical, and transcritical flow along coastal topography. *J. Atmos. Sci.*, **56**, 2780–2795, doi:10.1175/1520-0469(1999)056<2780:MSOSSA>2.0.CO;2.

Chao, Y., Z. Li, J. D. Farrara, and P. Huang, 2009: Blended sea surface temperatures from multiple satellites and in situ observations for coastal oceans. *J. Atmos. Oceanic Technol.*, **26**, 1415–1426, doi:10.1175/2009JTECHO592.1.

COESA, 1976: *U.S. Standard Atmosphere, 1976*. NOAA, 227 pp.

de Szoeke, S. P., S. Yuter, D. Mechem, C. W. Fairall, C. D. Burleyson, and P. Zuidema, 2012: Observations of stratocumulus clouds and their effect on the eastern Pacific surface heat budget along 20°S. *J. Climate*, **25**, 8542–8567, doi:10.1175/JCLI-D-11-00618.1.

Dorman, C. E., 1985: Evidence of Kelvin waves in California's marine layer and related eddy generation. *Mon. Wea. Rev.*, **113**, 827–839, doi:10.1175/1520-0493(1985)113<0827:EOKWIC>2.0.CO;2.

——, and C. D. Winant, 2000: The structure and variability of the marine atmosphere around the Santa Barbara Channel. *Mon. Wea. Rev.*, **128**, 261–282, doi:10.1175/1520-0493(2000)128<0261:TSAVOT>2.0.CO;2.

——, and D. Koračin, 2008: Response of the summer marine layer flow to an extreme California coastal bend. *Mon. Wea. Rev.*, **136**, 2894–2992, doi:10.1175/2007MWR2336.1.

——, D. P. Rogers, W. Nuss, and W. T. Thompson, 1999: Adjustment of the summer marine boundary layer around Point Sur, California. *Mon. Wea. Rev.*, **127**, 2143–2159, doi:10.1175/1520-0493(1999)127<2143:AOTSMB>2.0.CO;2.

Haack, T., S. D. Burk, C. Dorman, and D. Rodgers, 2001: Supercritical flow interaction within the Cape Blanco–Cape Mendocino orographic complex. *Mon. Wea. Rev.*, **129**, 688–708, doi:10.1175/1520-0493(2001)129<0688:SFIWTC>2.0.CO;2.

Koračin, D., and C. E. Dorman, 2001: Marine atmospheric boundary layer divergence and clouds along California in June 1996. *Mon. Wea. Rev.*, **129**, 2040–2056, doi:10.1175/1520-0493(2001)129<2040:MABLDA>2.0.CO;2.

Nuss, W. A., and Coauthors, 2000: Coastally trapped wind reversals: Progress toward understanding. *Bull. Amer. Meteor. Soc.*, **81**, 719–743, doi:10.1175/1520-0477(2000)081<0719:CTWRPT>2.3.CO;2.

Parish, T. R., 2000: Forcing of the summertime low-level jet along the California coast. *J. Appl. Meteor.*, **39**, 2421–2433, doi:10.1175/1520-0450(2000)039<2421:FOTSLL>2.0.CO;2.

——, M. D. Burkhart, and A. R. Rodi, 2007: Determination of the horizontal pressure gradient force using global positioning system onboard an instrumented aircraft. *J. Atmos. Oceanic Technol.*, **24**, 521–528, doi:10.1175/JTECH1986.1.

——, D. A. Rahn, and D. Leon, 2013: Airborne observations of a Catalina eddy. *Mon. Wea. Rev.*, **141**, 3300–3313, doi:10.1175/MWR-D-13-00029.1.

——, ——, and ——, 2014: Aircraft observations of the marine boundary layer adjustment near Point Arguello, California.

J. Appl. Meteor. Climatol., **53**, 970–989, doi:10.1175/JAMC-D-13-0164.1.

——, ——, and ——, 2015: Aircraft observations and numerical simulations of the developing stage of a southerly surge near Southern California. *Mon. Wea. Rev.*, **143**, 4883–4903, doi:10.1175/MWR-D-15-0140.1.

——, ——, and ——, 2016a: Aircraft measurements and numerical simulations of an expansion fan off the California coast. *J. Appl. Meteor. Climatol.*, **55**, 2053–2062, doi:10.1175/JAMC-D-16-0101.1.

——, ——, and ——, 2016b: Research aircraft determination of D-value cross sections. *J. Atmos. Oceanic Technol.*, **33**, 391–396, doi:10.1175/JTECH-D-15-0173.1.

Pomeroy, K. R., and T. R. Parish, 2001: A case study of the interaction of the summertime coastal jet with the California topography. *Mon. Wea. Rev.*, **129**, 530–539, doi:10.1175/1520-0493(2001)129<0530:ACSOTI>2.0.CO;2.

Rahn, D. A., and T. R. Parish, 2007: Diagnosis of the forcing and structure of the coastal jet near Cape Mendocino using in situ observations and numerical simulations. *J. Appl. Meteor. Climatol.*, **46**, 1455–1468, doi:10.1175/JAM2546.1.

——, and C. J. Mitchell, 2016: Diurnal climatology of the boundary layer in Southern California using AMDAR temperature and wind profiles. *J. Appl. Meteor. Climatol.*, **55**, 1123–1137, doi:10.1175/JAMC-D-15-0234.1.

——, T. R. Parish, and D. Leon, 2013: Coastal jet adjustment near Point Conception, California, with calm conditions in the bight. *Mon. Wea. Rev.*, **141**, 3827–3839, doi:10.1175/MWR-D-13-00030.1.

——, ——, and ——, 2014: Coastal jet adjustment near Point Conception, California, with opposing wind in the bight. *Mon. Wea. Rev.*, **142**, 1344–1360, doi:10.1175/MWR-D-13-00177.1.

——, ——, and ——, 2016: Observations of large wind shear above the marine boundary layer near Point Buchon, California. *J. Atmos. Sci.*, **73**, 3059–3077, doi:10.1175/JAS-D-15-0363.1.

Rogers, D. P., and Coauthors, 1998: Highlights of Coastal Waves 1996. *Bull. Amer. Meteor. Soc.*, **79**, 1307–1326, doi:10.1175/1520-0477(1998)079<1307:HOCW>2.0.CO;2.

Samelson, R. M., 1992: Supercritical marine-layer flow along a smoothly varying coastline. *J. Atmos. Sci.*, **49**, 1571–1584, doi:10.1175/1520-0469(1992)049<1571:SMLFAA>2.0.CO;2.

Wakimoto, R., 1987: The Catalina eddy and its effect on pollution in Southern California. *Mon. Wea. Rev.*, **115**, 837–855, doi:10.1175/1520-0493(1987)115<0837:TCEAIE>2.0.CO;2.

Wang, Z., P. Wechsler, W. Kuestner, J. French, A. Rodi, B. Glover, M. Burkhart, and D. Lukens, 2009: Wyoming cloud lidar: Instrument description and applications. *Opt. Express*, **17**, 13 576–13 587, doi:10.1364/OE.17.013576.

——, and Coauthors, 2012: Single aircraft integration of remote sensing and in situ sampling for the study of cloud microphysics and dynamics. *Bull. Amer. Meteor. Soc.*, **93**, 653–668, doi:10.1175/BAMS-D-11-00044.1.

Winant, C. D., C. E. Dorman, C. A. Friehe, and R. C. Beardsley, 1988: The marine boundary layer off northern California: An example of supercritical channel flow. *J. Atmos. Sci.*, **45**, 3588–3605, doi:10.1175/1520-0469(1988)045<3588:TMLONC>2.0.CO;2.

Zemba, J., and C. A. Friehe, 1987: The marine boundary layer jet in the coastal ocean dynamics experiment. *J. Geophys. Res.*, **92**, 1489–1496, doi:10.1029/JC092iC02p01489.